

REAL-TIME EMULATION TESTBENCH FOR FUEL-CELL/BATTERY HYBRIDIZATION IN HYDROGEN-ELECTRIC AVIATION

Gianluca Marinaro[1], Clemente Serpico[1], Luca Garbarino[1], Michele Inverno[1], Giulia Malaponte[1], Antonio Bono[1] & Antonio Pagano[1]

[1]CIRA, Via Maiorise, SNC, 81043 Capua, ITALY.

Abstract

Electrification and hydrogen technologies are emerging as synergistic solutions to advance aviation sustainability and abate local carbon emissions. They address current technological gaps by leveraging the high specific energy of hydrogen alongside the operational efficiency of electric motors. In the short-range sector, battery-powered flights are technically proven for general aviation and air taxi operations but limited by slow scalability and battery maturity. Developers of regional aircraft and advanced air mobility (AAM) platforms are increasingly prioritizing hydrogen-electric propulsion, driven by its superior energy density, which enables extended range and higher payload capacities. In parallel, hydrogen combustion is attracting renewed interest, shifting the focus toward resolving storage and safety complexities. Within this context, CIRA's Electroplane project ("Electric and Hybrid-Electric Aircraft - Maturation of Innovative Technologies"), launched in 2021, aims at consolidating technologies for low-emission air transportation, as a part of a long-term transition to zero emissions.

This work reports the first operational phase of the project, focused on a laboratory emulation environment where programmable power hardware reproduces the dynamic behavior of a hydrogen-electric aircraft powertrain based on a fuel-cell system and a battery pack, while the propulsive load is emulated by a third bidirectional unit. The bench is based on ITECH IT6018B-1500-40 regenerative DC power units, showing up to 18 kW power, 0–1500 V output range, and ±40 A capability. MATLAB/Simulink® numerical models, validated against experimental data, are executed in real time to drive the emulators as physics-based electrochemical sources under mission transients. A dedicated communication architecture enables closed-loop testing of energy management strategies and fault scenarios prior to the integration of real electrochemical sources.

Keywords: Hydrogen-electric propulsion, Energy management system (EMS), Hardware-in-the-loop (HIL), Fuel cell-battery hybridization.

1. Introduction

Numerous initiatives around the world are being launched to experimentally demonstrate the technical feasibility of aeronautical propulsion systems that mitigate environmental impacts. The ability to move from concept to design, through experimental validation, requires the availability of adequate infrastructure. Investments are often substantial, so these infrastructures must be flexible enough to ensure their use beyond initial applications, allowing them to be reconfigured and accommodate broader experimentation. Test benches for electric or hybrid-electric propulsion systems with power outputs in the order of several megawatts are very expensive, which implies high costs for research institutes if end-users are not expected to be committed for a long time. Very often proprietary test benches are an integral part of the equipment that new operators, such as Zeroavia or Vertical Aerospace, take into consideration from the early stages of aircraft development. On the other hand, affordable research test benches for propulsion system demonstrators with significantly lower power levels must be designed to support the upscaling of the tested technologies.

Based on these considerations, a plan was defined for the construction of test benches at CIRA aimed at validating electric and hybrid-electric propulsion technologies. The activity starts with a small bench capable of reaching up to 100 kW intended for the maturation and experimentation of technologies that can be scalable to higher power levels. This test bench is specifically designed to investigate hydrogen-electric propulsion systems, thanks to its modular architecture that allows the use of both emulated and real electrochemical sources and electrical loads as components.

Hydrogen-electric propulsion promises to replace combustion engines of equal power, especially for short-haul and regional commercial flights, enabling zero local carbon emissions [1]. In many configurations, hydrogen is converted to electricity through a fuel-cell system and supplied to the electrical propulsion system, typically supported by a battery pack that provides buffering, peak shaving, and improved dynamic response. The combined adoption of fuel-cells and batteries is aimed not only at meeting transient power demands, but also at managing multiple operational constraints and trade-offs, including fuel-cell voltage/current operating limits, compressor performance maps for the fuel-cell, transient capability, battery state-of-charge boundaries, and thermal management requirements [2].

However, the development and validation of these systems show a few challenges: simulation approaches often fail to capture real-world constraints, while full-scale experimental facilities, as discussed above, are costly, complex, and less flexible. Hardware-in-the-Loop (HIL) or Power-Hardware-in-the-Loop (PHIL) methodologies have emerged as an promising solution, integrating real hardware components with real-time simulation models and providing a controlled environment for system-level validation.

In the context of hybrid electric propulsion systems, numerous studies have demonstrated the effectiveness of HIL methodologies. Real-time emulation of fuel-cell electric vehicle (FCEV) powertrains has been used to support the development of advanced control strategies, such as model predictive control implementations [3]; real-time platforms have been also used to validate energy management strategies in order to optimize power allocation between multiple energy sources [4] or HIL platforms have been applied to the validation of battery models and control algorithms under real dynamic conditions [5]. HIL techniques can significantly reduce development time and experimental costs, improving safety by enabling the testing of control strategies under critical or fault scenarios that would be difficult to reproduce in full-scale experiments.

Despite the extensive adoption of HIL or PHIL methodologies in the automotive field [6], [7], their application to aeronautical hybrid electric propulsion systems remains limited [8],[9]. This gap motivates the development of dedicated PHIL platforms capable of emulating the interaction between multiple energy sources under operating conditions.

This work presents a PHIL platform designed for the emulation and testing of an electric propulsion system based on a hybrid fuel-cell and battery architecture. The setup uses multiple programmable power supply emulators with real-time models developed in Simulink, allowing for representation of system dynamics and control strategies under realistic operating conditions for aircraft.

The main contribution of this paper is threefold. First, a modular PHIL architecture for multi-source electric propulsion systems is developed. Second, models of the fuel-cell, battery and control system are implemented and executed in real time. Third, the platform is experimentally assessed under both nominal and fuel-cell failure conditions, demonstrating its capability to reproduce source reconfiguration and power-sharing transient relevant to aeronautical applications.

The paper structure is the following: section 2 describes system architecture, section 3 presents the battery and fuel-cell models, section 4 specifies the control strategy, section 5 specify the test case, and section 6 reports the experimental results.

2. System architecture

2.1 System description and hardware setup

The proposed system is a Power-Hardware-in-the-Loop (PHIL) platform designed for the real-time emulation and validation of a hybrid-electric propulsion system for aeronautical applications. As shown in Figure 1, the architecture uses three programmable DC power supply emulators that represent fuel-cell, battery, and load and a real-time target machine implementing system models

and control algorithms. Two host computers are dedicated to supervisory control and Human Machine Interface (HMI) functionalities.

The power stage is based on ITECH IT6018B programmable DC power supplies that can operate in voltage, current, and power control modes over a wide range (up to 1500 V and 40 A). The fast dynamic response, combined with programmability using SCPI commands, allows precise reproduction of the nonlinear electrical behavior of both fuel-cell and battery systems without dedicated physical prototypes, maintaining the fidelity of the emulated electrical characteristics under dynamic load conditions representative of real flight profiles.

Real-time calculation is performed by a dedicated target machine operating at a fixed sampling frequency of 25 Hz, representing a trade-off between model accuracy and computational load, ensuring deterministic execution of both simulation models and control algorithms within real-time constraints. Host systems, instead, aren't subject to strict timing requirements and thus operate at a lower update rate of 10 Hz.

From a communication viewpoint, in the architecture two complementary protocols are adopted to meet the different layer-specific interface needs. UDP is used for data exchange between the real-time target and the host computers due to its low latency and minimal overhead; TCP/IP is employed for communication with the power supply units, offering reliable, connection-oriented data transfer suitable for hardware command and measurement exchange. A dedicated interface computer is integrated as a protocol bridge between these two communication layers, decoupling the real-time environment from the hardware interface and improving overall system robustness without introducing additional signal processing.

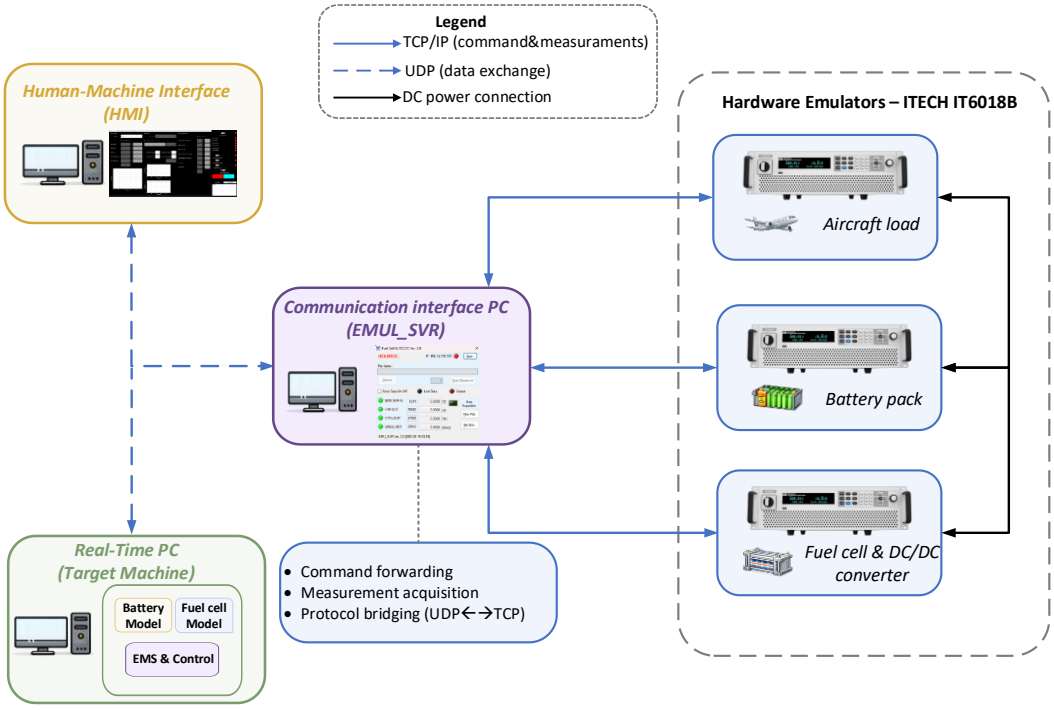


Figure 1 – Simplified architecture of the proposed PHIL platform, including the real-time target, HMI, communication interface, and programmable power supply emulators.

2.2 Software architecture

The core of the system is a real-time model developed in Simulink environment and executed on a real-time target machine using a single-task scheduling approach. The whole model, including fuel-cell and battery systems, stateflow-based control algorithms, is performed at fixed sampling frequency, guaranteeing deterministic behavior and tight coupling between control decisions and system response.

The real-time model integrates both the component-level simulations and the control strategy.

Battery models compute the DC bus voltage based on system conditions, while the control algorithm defines the operating mode and generates the setpoint current for the fuel-cell DC/DC converter. The load power is acquired from the load emulator, which is determined according to a mission profile defined by the Human-Machine Interface (HMI).

At each sampling step, the real-time system runs a cyclic sequence of operations. First, measurement data from the hardware emulators are acquired; then, the system states and control logic are updated, and new reference signals are calculated. The battery model updates the bus voltage – and the emulated battery power supply - while the control system generates the current setpoint for the fuel-cell emulator. These signals are transmitted to the hardware layer for actuation.

Communication interface PC (EMUL_SVR) is a dedicated interface node located on the shared LAN. The EMUL_SVR operates as a bidirectional protocol bridge: on its software-facing side, it receives high-level control setpoints from the real time PC via UDP, at rates dictated by the real-time model cycle (up to 25 Hz); on its hardware-facing side, it maintains three independent persistent TCP/IP connections to the ITECH IT6018B units (one per emulated source), over which it issues SCPI commands to configure and actuate each power supply. This architectural separation is intentional: the non-deterministic latency inherent to TCP transactions with physical hardware is absorbed and isolated within the EMUL_SVR, so that it never propagates back into the real-time simulation loop running on the real-time PC.

The EMUL_SVR translates each setpoint from real time models into the appropriate SCPI instruction and transmits it to the target hardware unit over TCP. Conversely, measurement data acquired from the power supplies are encapsulated by the EMUL_SVR into housekeeping packets and deliver them at 10 Hz to both the real time PC and the HMI, closing the feedback loop and supplying the simulation models with physically grounded measurements, Figure 2.

The Human-Machine Interface (HMI) is the supervisory layer, providing real-time visualization of system variables and enabling user interaction. In addition to monitoring, the HMI allows on-line modification of control parameters, such as fuel-cell power limits, battery constraints, operational thresholds and battery parameters data, such as initial SoC, number of series and parallel cells. Another function is to define mission profiles, including load power and altitude trajectories, and supports system-level commands such as start-up, shutdown, and emergency handling. Furthermore, logging and fault monitoring functionalities are implemented to support experimental analysis, Figure 2.

The overall software architecture incorporates a timestamp-based synchronization mechanism, ensuring that all log data, spanning from high-level HMI commands to low-level hardware measurements, can be accurately correlated during post-processing and fault analysis

The proposed architecture allows continuous bidirectional interaction between simulated models and physical hardware components. The separation between real-time computation, communication management, and supervisory control ensures modularity and flexibility to test different system configurations and control strategies, facilitating future extensions.



Figure 2 – Human-Machine Interface (HMI) and EMUL_SVR software for real-time monitoring, mission profile configuration, supervisory control, and data exchange of the PHIL platform.

2.3 Communication protocol and data exchange

To support the multi-subsystem integration, a custom message-based protocol has been designed and implemented over UDP, with a complementary TCP layer reserved for hardware actuation. The protocol defines a uniform packet structure applicable to all software-layer exchanges, regardless of message direction or content type.

Each packet conforms to a fixed seven-field format, as illustrated in Figure 3. The frame opens with a synchronization delimiter (0xAA) and closes with an end delimiter (0xEE), enabling reliable boundary detection even in the presence of buffer misalignment. A one-byte length field (LenStream) allows receivers to pre-allocate buffer space and verify packet completeness prior to parsing. The *"Source"* field identifies the originating subsystem, enabling proper message routing in a multi-participant network. The *"MsgType"* field determines the structure of the variable-length payload (Stream), which ranges from 0 to 235 bytes depending on message function. A UTC timestamp, encoded as an IEEE 754 double-precision value, is embedded in every packet, providing a common temporal reference for synchronization across subsystems and for post-test log reconstruction.

All messages are organized into three priority classes, as shown in Figure 3. Critical messages (0xC0–0xCF) handle emergency conditions and safety-critical commands; these require immediate processing and preempt lower-priority traffic. High-priority messages (0xD0–0xDF) carry configuration parameters and real-time control setpoints, as well as mission and control parameter uploads issued by the HMI. Response messages (0xA0–0xAF) carry acknowledgements and periodic housekeeping messages from both the emulation server and the simulation models.

At the hardware interface layer, the EMUL_SVR translates the received UDP setpoints into SCPI commands transmitted over dedicated TCP connections, one per emulator unit. This layer is intentionally kept separate from the UDP protocol: the connection-oriented nature of TCP guarantees delivery of hardware commands where packet loss is not acceptable, while the UDP protocol retains the low-latency, stateless behavior required by the real-time control loop.

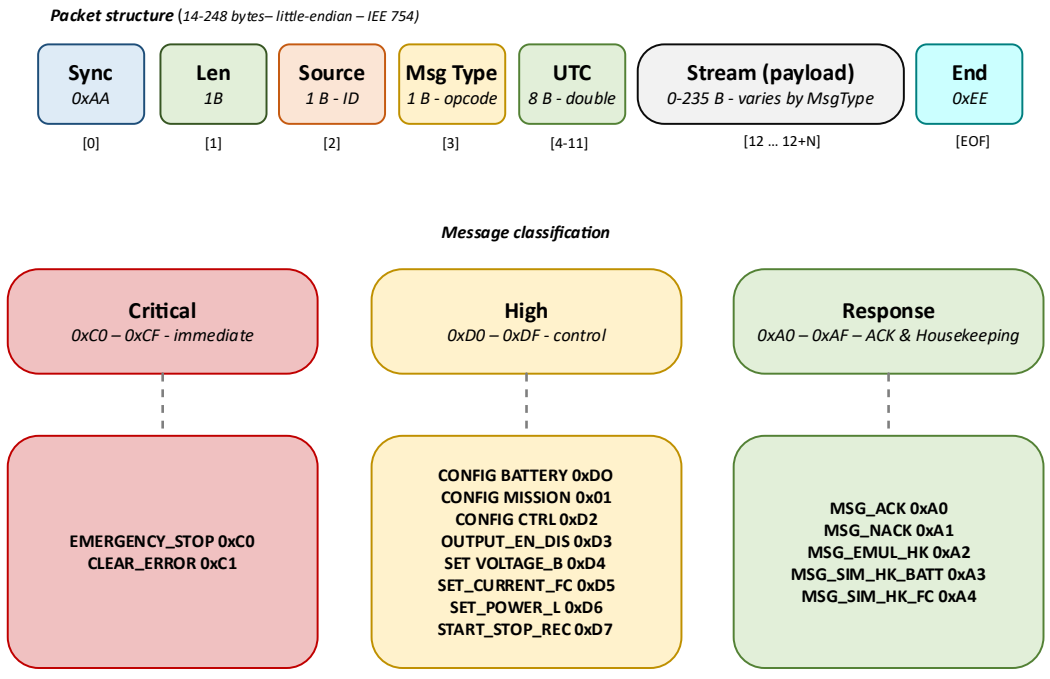


Figure 3 – Packet structure and message classification of the proposed PHIL platform.

3. Energy source modeling

In the proposed propulsion system, Proton Exchange Membrane Fuel-cell (PEMFC) serves as the primary energy source, ensuring the power demand during cruise operating conditions. Battery packs act as secondary energy sources, providing dynamic power support during rapid transients

and functioning as energy buffers to enhance system responsiveness and stability. The modeling approaches adopted for both energy sources are presented in this section and discussed in detail in the following subsections.

3.1 Battery model

A modular battery model has been designed in Simulink to accurately represent the electrical and thermal behavior of the battery system within the proposed PHIL platform. The model, based on equivalent circuit approach, has been developed to provide a realistic representation of the dynamics of the battery pack, yet computationally efficient to be used in real-time applications.

A second-order equivalent circuit model (ECM) composed of an open-circuit voltage source, a series of internal resistance, and two RC branches are employed to describe the electrical characteristics of a single battery cell [10]. This configuration enables the steady state response and the transient electrochemical dynamics of the cell to be reproduced during charge and discharge conditions.

The cell terminal voltage can be expressed as:

$$V_{cell} = OCV(SoC, T) - I_{cell}R_0 - V_1 - V_2 \quad (1)$$

where $OCV(SoC, T)$is the open-circuit voltage as a function of the state of charge and temperature, R_0 is the ohmic internal resistance, and $V_1$and V_2represent the voltage of the two RC branches related to polarization and diffusion effects.

The dynamic of each RC branch is governed by the following equation:

$$\frac{dV_n}{dt} = \frac{I_{cell}}{C_n} - \frac{V_n}{R_n C_n}, n \in \{1,2\} \quad (2)$$

where $R_n$and $C_n$are the resistance and capacitance values of the corresponding RC branch.

The parameters of the equivalent circuit model have been identified for different battery chemistries through optimization procedures of experimental data [11] and reference values obtained from literature [12],[13]. The platform supports a wide range of cell technologies such as Lithium Iron Phosphate (LFP), Nickel Manganese Cobalt Oxide (NMC) and Lithium Titanate Oxide (LTO). The user can select the desired cell type directly from the HMI, allowing for a rapid reparameterization of the battery model based on the application scenario under analysis.

Starting from the single-cell model, the whole pack is generated from the single cell model according to the number of cells connected in series and parallel. These parameters can be configured from the HMI, so that battery packs with different voltage and capacity ratings can be simulated. The pack output voltage and capacity are:

$$V_{pack} = N_s V_{cell} \quad (3)$$
$$C_{pack} = N_p C_{cell}$$

where $N_s$and N_p are the number of series and parallel cells, respectively.

The battery state of charge is estimated using the Coulomb counting method:

$$SOC(t) = SOC_0 - \frac{1}{C_{nom}} \int_0^t I_{cell}(\tau) d\tau \quad (4)$$

where C_{nom} is the nominal cell capacity and SOC_0 is the initial state of charge, which can be defined by the user through the HMI.

In addition to the electrical model, a simplified thermal model was also implemented to reproduce the pack temperature evolution during operation. The thermal behavior of each cell is modeled with an energy balance considering internally generated heat, conductive heat transfer with adjacent cells and convective heat transfer with ambient air and the liquid cooling system [14].

The temperature evolution of each cell is given by:

$$C_{th} \frac{dT_i}{dt} = Q_{gen} - Q_{cond} - Q_{air} - Q_{liq} \quad (5)$$

where C_{th} is the thermal capacitance of the cell, Q_{gen} is the internally generated heat, Q_{cond} is conductive heat exchange with adjacent cells, Q_{air} is the convective heat transfer with ambient air,

and Q_{liq} is the heat removed by the liquid cooling system.

Thermal coupling between neighboring cells is calculated as:

$$Q_{cond} = \sum_{j} g_{cond}(T_i - T_j) \tag{6}$$

where $g_{cond}$is the equivalent thermal conductance between adjacent cells.

The convective heat transfer with the liquid cooling channels is expressed as:

$$Q_{liq} = h_{liq} A_{liq} (T_i - T_{fluid}) \tag{7}$$

where h_{liq} is the convective heat transfer coefficient, A_{liq} is the contact area between the cell and the cooling channel, and T_{fluid} is the coolant temperature.

The liquid cooling system is composed of serpentine channels located every two cell strings. The convective heat transfer coefficient is dynamically adjusted to the coolant flow conditions based on Reynolds and Nusselt correlations:

$$Re = \frac{\rho v D_h}{\mu} \tag{8}$$

$$Nu = 1.87 \left(\frac{Re\ Pr\ D_h}{L} \right)^{1/3}$$

This thermal formulation enables the evaluation of temperature gradients within the battery pack and the analysis of thermal constraints under high power operating conditions.

Although the thermal model parameters were identified from literature data, uncertainties associated with quantities such as thermal contact conductance, convective heat transfer coefficients, and material thermal properties may affect the predicted temperature distribution. The proposed model is completely parameterized and can be easily extended to perform sensitivity and uncertainty analysis to evaluate the effect of parameter variations on the thermal behavior of the battery pack. Such investigations are seen as part of the future developments of the platform.

3.1.1 Battery model validation

The electrical parameters of the proposed battery model were identified and subsequently validated using experimental data available in the literature for an NMC cell. A Hybrid Pulse Power Characterization (HPPC) test was used for the estimation of equivalent circuit model parameters, while an independent dynamic driving cycle was used to verify the predictive capability of the identified model under continuously varying load conditions. The HPPC profile provides a sequence of current pulses over different state-of-charge levels, allowing the open-circuit voltage characteristic and the equivalent circuit parameters to be estimated. The parameters were obtained by fitting the model voltage response to the experimental terminal voltage during the pulse and relaxation phases. Therefore, the HPPC test was used as the identification dataset rather than as an independent validation case. The results obtained during the HPPC-based identification procedure are shown in Figure 4(a). The upper subplot compares the experimental terminal voltage with the voltage predicted by the identified numerical model. The middle subplot reports the corresponding voltage error together with the applied HPPC current profile, while the lower subplot shows the estimated battery state of charge. A close agreement between the experimental data and the numerical model is observed throughout the HPPC test, with voltage discrepancies generally lower than 50 mV for SoC values above 10%. Larger deviations occur near the end-of-discharge region, where the voltage-SoC characteristic becomes strongly nonlinear and more sensitive to parameter uncertainties and modeling assumptions.

After parameter identification, the model was validated against a dynamic driving cycle not used during the fitting process. This second dataset is characterized by continuously varying current demand and therefore provides a more representative assessment of the model capability under dynamic operating conditions. The validation results are shown in Figure 4(b). The simulated voltage closely follows the experimental voltage over the full discharge profile. Small discrepancies are observed during fast current transients and near the end-of-discharge region, where nonlinear

effects and parameter sensitivity become more pronounced. Nevertheless, the overall agreement confirms that the identified ECM parameters provide a satisfactory representation of the battery electrical behavior for the mission-level real-time applications considered in this work.

Although the thermal model is included in the real-time framework, the present experimental campaign focuses on electrical power-sharing dynamics. Thermal validation will be addressed in future work.

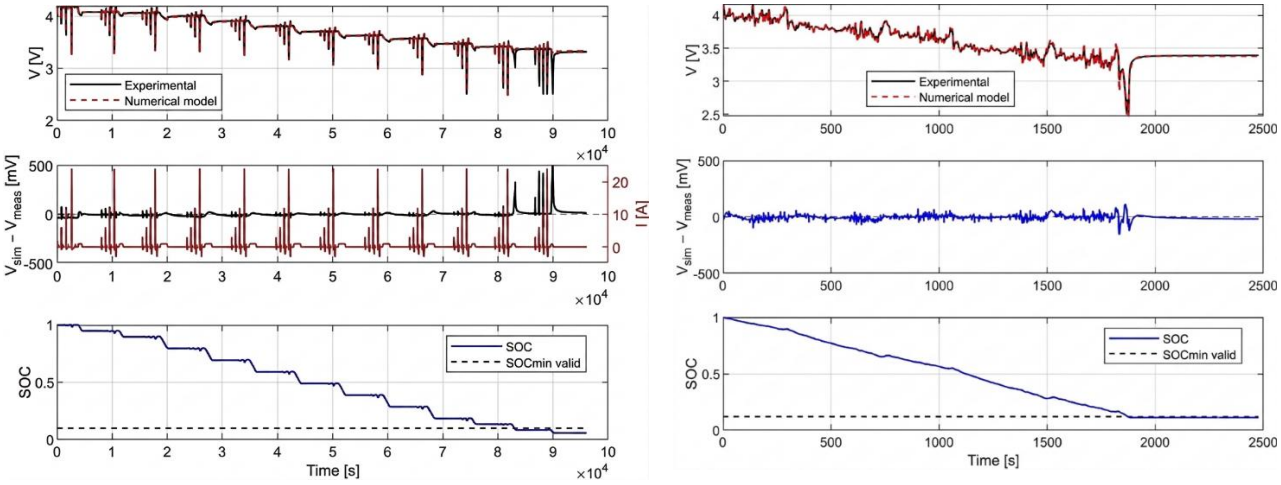


Figure 4 – Battery model parameter identification and validation: (a) HPPC cycle used to estimate electrical ECM parameters; (b) dynamic driving cycle used for independent validation of the identified parameters.

3.2 Fuel-cell model

The voltage of a single fuel-cell can be determined by accounting for various electrochemical losses, as expressed by the following equation:

$$U_{cell} = E_{Nernst} - V_{act} - V_{ohm} - V_{con} \tag{9}$$

In this expression, E_{Nernst} is the open-circuit voltage obtained from the Nernst equation, while V_{act}, V_{ohm}, and V_{con} represent the activation, ohmic, and concentration overpotentials, respectively. These terms collectively account for the voltage losses that occur during real-world fuel-cell operation.

The activation loss is evaluated using the following equation, which also accounts for concentration losses, which is not considered in the above equation:

$$V_{act} = B_1 + B_2 T + B_3 T ln\left(c_{O_2}\right) + B_4 T ln(j) \tag{10}$$

where B_1, B_2, B_3, B_4 are empirical coefficients determined from experimental calibration.

Finally, ohmic loss is determined by

$$V_{ohm} = j(R_{ohm} + R_c) \tag{11}$$

Here, R_c represents the contact or electronic resistance (typically assumed as 0.008 Ω·cm²), while the protonic resistance of the membrane, R_{ohm}, is defined by the ratio t_m/σ_m, where t_m denotes the membrane thickness and σ_m is the membrane's ionic conductivity, which varies with water content and temperature.

The input partial pressures of hydrogen and oxygen can be modeled as:

$$p_{H_2} = 0.5 p_{H_2O}^{sat} \left[exp\left(\frac{1.635j}{T^{1.334}}\right)\left(\frac{p_a}{p_{H_2O}^{sat}}\right)\right] \tag{12}$$

$$p_{O_2} = p_{H_2O}^{sat} \left[exp\left(\frac{4.192j}{T^{1.334}}\right)\left(\frac{p_c}{p_{H_2O}^{sat}}\right)\right]$$

In this context, j denotes the current density measured in [A/cm²], p_a and p_c represent the partial pressures at the anode and cathode, respectively, and p_{H_2O} refers to the partial pressure of water vapor in the fuel-cell system.

3.2.1 Fuel-cell model validation

To assess the accuracy of the proposed fuel-cell model, its predictions were compared against experimental polarization and power characteristics available in the literature for the selected fuel-cell. The validation dataset covers the full operating current range and is widely used as a benchmark for model development and parameter identification.

Figure 5 shows both the comparison between the simulated and reference polarization curves and the simulated and experimental power-current characteristics. A good agreement is observed over the whole range of operation. This shows that the model correctly reproduces the drop in voltage when the demand for current increases. The usual activation, ohmic and concentration loss regions are properly identified, demonstrating the suitability of the adopted model for real time applications. The simulated power output is also in good agreement with the reference experimental data, correctly reproducing the rise of the power at low and medium current levels and the saturation behavior at higher currents.

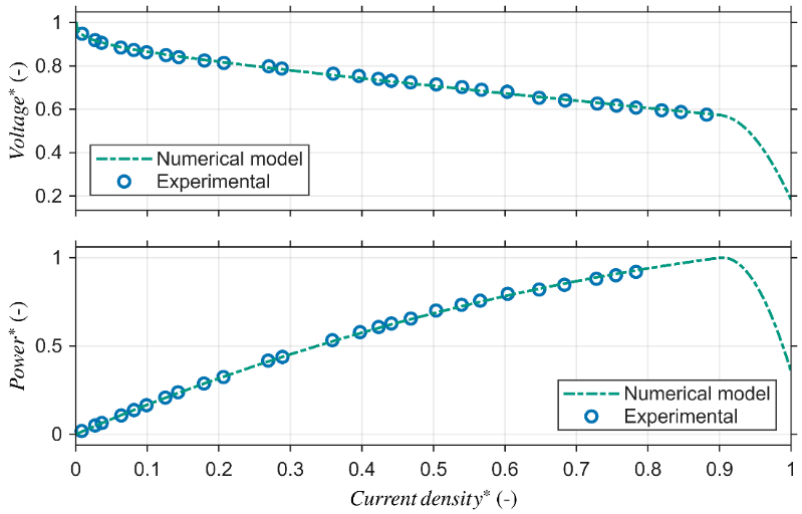


Figure 5 – Dimensionless polarization and power curves for the fuel-cell.

4. Control strategy

4.1 Power and energy management strategy

Energy management system (EMS) plays a central role in hybrid-electric propulsion system coordinating the power and energy interaction between the electrical source (fuel-cell and battery in this case) and load and facilitating the efficient distribution of power. The main objectives of the EMS are to ensure efficient utilization of the fuel-cell, maintain the battery state of charge within a predefined operating range, guarantee stable operation under variable load conditions, and preserve component lifetime by enforcing operational limits such as battery C-rate and temperature constraints.

Different energy management strategies for hybrid-electric energy systems, usually classified into two main categories, have been proposed in literature: rule-based and optimization-based methodologies. Rule-based strategies, such as deterministic state machine or fuzzy logic, are commonly adopted due to their simplicity, robustness, and suitability for real-time implementation, although they don't guarantee global optimality. Optimization-based methods, on the other side, aim to improve system efficiency but usually need accurate system models and higher computational effort. More advanced approaches, such as Model Predictive Control (MPC), enable optimal power allocation while explicitly handling system constraints, at the cost of increased computational complexity and potential challenges in real-time implementation [15].

In the context of Hardware-in-the-Loop applications and real-time validation, rule-based approaches remain particularly attractive due to their low computational cost, ease of implementation, and robustness.

Based on these considerations, the proposed EMS is employed using a rule-based strategy. The adopted approach is based on a finite state machine developed in MATLAB Stateflow, which determines the system operating mode as a function of the load power demand P_{load}, the battery and fuel-cell state, and the system constraints.

Supervisory control generates two discrete command signals:

$$FC_{cmd}, BATT_{cmd} \in \{-1,0,1\} \tag{13}$$

which defines the desired operating condition of the fuel-cell and the battery. These signals are mapped into continuous control action through a rule-based mapping implemented via a truth table, which provides the reference current for the fuel-cell DC/DC converter.

The power balance of the system can be expressed as:

$$P_{load} = \eta_{dc} P_{fc} + P_{batt} \tag{14}$$

where the fuel-cell contribution is actively controlled, while the battery compensates for the remaining power according to the system dynamics.

The state machine defines several operating modes to manage the system under different conditions. In the Idle state, corresponding to negligible load demand, the fuel-cell operates in idle conditions while the battery may be recharged if required. In the Supply state, when the load demand is lower than the maximum fuel-cell capability and the battery state of charge is within its operating range, the fuel-cell supplies the entire load. In the Max Power state, when the load demand exceeds the fuel-cell capability, the fuel-cell operates at its maximum output power, and the battery provides the additional power required.

When the battery state of charge falls below a minimum threshold, charging conditions are enforced. In the Supply & Charge state, the fuel-cell simultaneously supplies the load and charges the battery, while in the Charge state, activated when no load is present, the fuel-cell is exclusively used to recharge the battery. Additional fault states are defined to handle abnormal conditions such as battery overtemperature, excessive charge/discharge rates, or fuel-cell limitations, ensuring safe system operation. The overall state machine structure is illustrated in Figure 6.

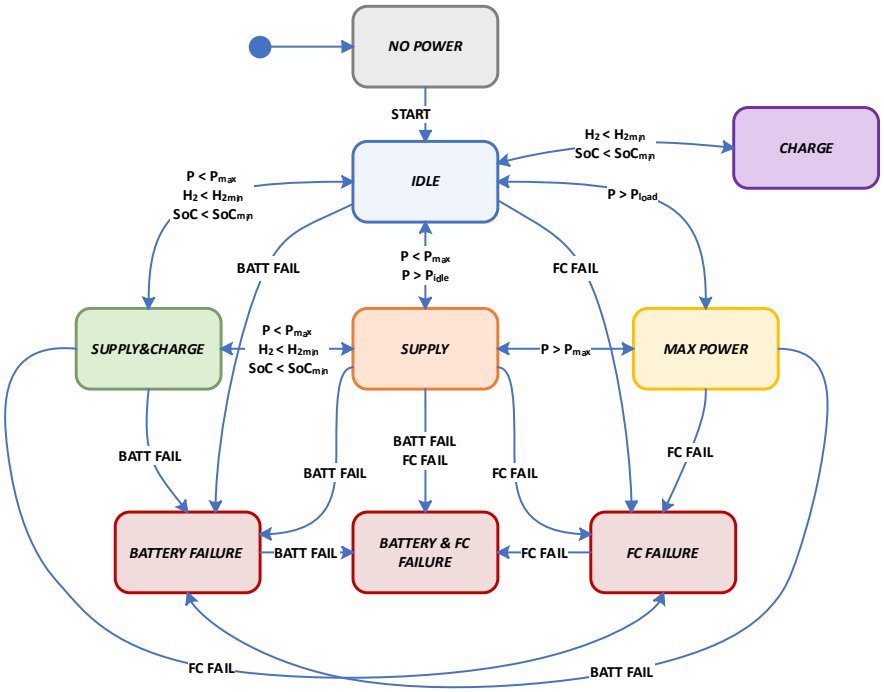


Figure 6 – Stateflow-based finite state machine implementing the control strategy.

The transitions between operating modes are governed by threshold-based conditions designed to avoid undesired oscillations and ensure smooth switching. The control parameters defining these thresholds, including fuel-cell power limits, hydrogen availability, battery constraints, and state-of-charge bounds, can be adjusted through the Human-Machine Interface (HMI).

The low-level control action is implemented by regulating the reference current of the fuel-cell DC/DC converter, which determines the fuel-cell power contribution. This relationship can be expressed as:

$$I_{fc} = f(FC_{cmd}, BATT_{cmd}, P_{load}, battery\ parameters, fuel\ cell\ parameters) \quad (15)$$

where the function f represents the mapping defined in the truth table. The battery is not directly controlled, but its behavior is governed by a real-time model that imposes the DC bus voltage, allowing it to naturally compensate for power imbalances.

The proposed control strategy provides a simple yet effective solution for real-time energy management, making it particularly suitable for Hardware-in-the-Loop implementation and experimental validation.

5. Test cases description

The experimental activity was carried out by considering two representative mission profiles, both defined through the HMI and executed on the proposed PHIL platform. The objective of the tests was to assess the capability of the real-time emulation environment to reproduce the dynamic interaction between the fuel-cell system, the battery pack, and the propulsive load under nominal and degraded operating conditions. The same mission profile structure was used in both cases. The profile includes the time history of the requested load power and the altitude, which are imposed as external mission inputs to the real-time model. The load power demand is reproduced by the load emulator, while the altitude profile is used by the fuel-cell model to account for the effect of operating conditions on the fuel-cell system response.

The first test case corresponds to a standard mission, visible in Figure 7, in which the hybrid powertrain operates without faults. In this condition, the fuel-cell is expected to act as the primary energy source during the cruise phase, while the battery provides transient support, peak-shaving capability, and power compensation during rapid variations of the load demand.

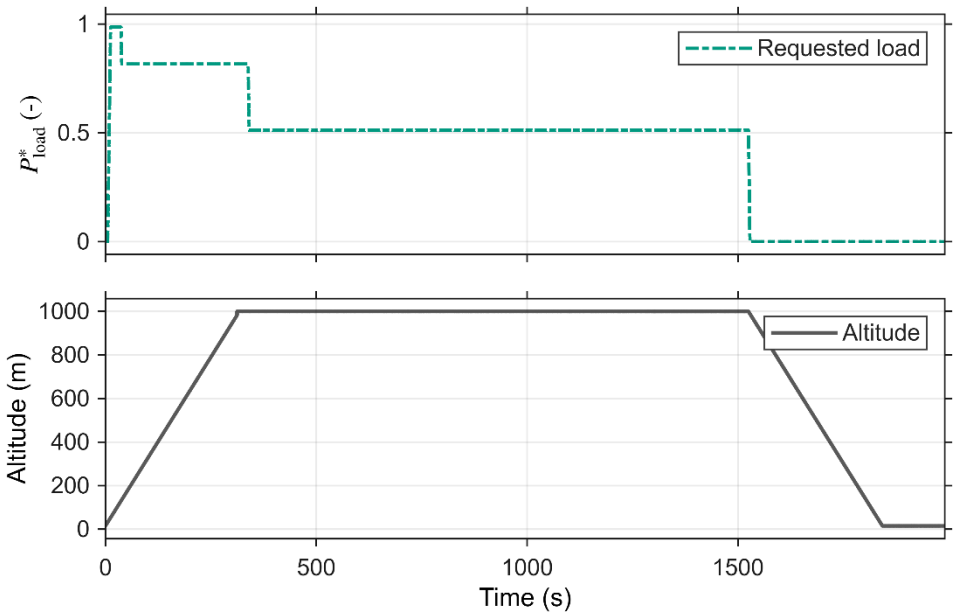


Figure 7 – Mission profile for the standard mission: requested load power and altitude profile.

The second test case, presented in Figure 8, introduces a fuel-cell failure during the mission. This scenario represents a degraded operating condition in which the fuel-cell contribution is partially reduced or completely lost during flight. Consequently, the energy management system is required to reconfigure the power split between the sources, forcing the battery to recover the role of primary

power source during the cruise phase. This test is particularly relevant to evaluate the robustness of the control strategy and the ability of the PHIL platform to reproduce fault-induced transients in a safe and repeatable laboratory environment.

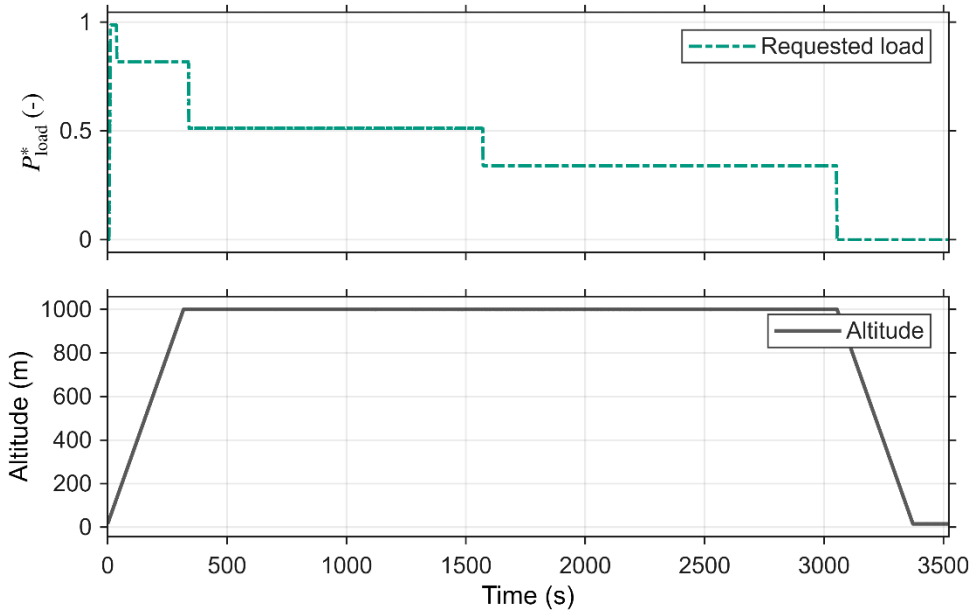


Figure 8 – Mission profile for the fuel-cell failure mission: requested load power and altitude profile.

For both mission profiles, three different signal sources, when available, are compared in the figures presented in the next section to support the discussion of the results: the offline Simulink model, the model executed on the real-time PC, and the electrical quantities measured from the hardware emulators. This comparison allows the verification of the consistency between the numerical model, the real-time implementation, and the physical emulation layer. Power, voltage, and current are reported in dimensionless form to facilitate comparison between subsystems and operating conditions. The time axis is kept dimensional to preserve the temporal interpretation of the mission events.

6. Results and discussion

The results are organized according to the two mission profiles described in Section 5. For each case, the requested mission profile is first considered in terms of load power and altitude. Then, the dynamic response of the hybrid powertrain is analyzed through the comparison of power, voltage, current, battery state of charge, and hydrogen consumption.

The comparison between the offline Simulink model and the real-time PC model is used to verify the correct deployment of the models in the real-time environment. The comparison with the hardware emulator measurements is instead used to assess the capability of the PHIL platform to reproduce the commanded electrical behavior at the power interface. Small discrepancies between numerical and measured quantities are expected due to communication delays, sampling frequency differences, internal control dynamics of the programmable DC units, and measurement filtering.

6.1 Standard

The standard mission represents the nominal operating condition of the hybrid fuel-cell/battery powertrain. During the mission, the energy management system assigns the fuel-cell the role of primary energy source, especially during the cruise phase, whereas the battery mainly supports transient events and compensates for the difference between the load demand and the fuel-cell power contribution.

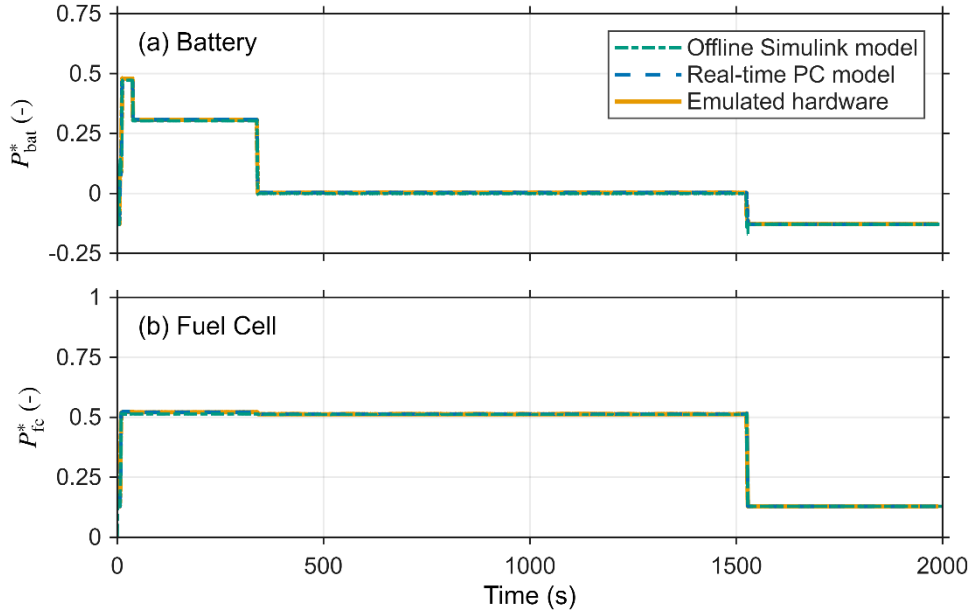


Figure 9 – Power comparison in the "Standard Mission".

The power comparison in Figure 9 shows a good agreement between the offline Simulink model, the real-time PC model, and the hardware emulator measurements. The dimensionless root-mean-square-error $RMSE^*$ was computed for each quantity over the common time interval of the compared signals. For the battery and the fuel-cell power, the offline Simulink model and the real time PC implementation show a close agreement, with $RMSE^*_{off-rt} = 0.59\% \; and \; 0.54\%$ respectively. The discrepancies between the real-time PC model and the hardware emulator are lower, equal to $RMSE^*_{rt-hw} = 0.16\%$ and 0.23% for the battery and the fuel-cell, confirming the ability of the hardware layer to accurately reproduce the real-time model commands. The fuel-cell power follows the main load demand during the quasi-steady portions of the mission, confirming that the EMS correctly prioritizes the fuel-cell system as the main source under nominal conditions. The battery power remains lower on average and becomes more significant during transient phases, where it contributes to power balancing and improves the dynamic response of the hybrid system.

In the final part of the mission, the requested load power decreases below the minimum idle operating power of the fuel-cell. In this condition, the fuel-cell is not switched off, since frequent shutdown and restart operations are generally undesirable for this type of system due to slow transient response, auxiliary management requirements, and potential degradation associated with repeated cycling. Therefore, the fuel-cell is kept operating at its minimum stable power level, and the surplus power is used to recharge the battery. This behavior is visible in Figure 9, where the battery power becomes negative according to the adopted sign convention, indicating that the battery is absorbing power rather than delivering it.

The voltage plots, visible in Figure 10, confirm the consistency of the real-time implementation with respect to the offline model. For the battery subsystem, the voltage measured at the emulator follows the model predictions with limited deviations, showing that the emulator is able to reproduce the dynamic voltage behavior imposed by the real-time battery model ($RMSE^*_{off-rt} = 0.05\% \; and \; RMSE^*_{rt-hw} = 0.04\%$). For the fuel-cell subsystem, the comparison is limited to the offline and real-time PC models because the available hardware voltage is measured downstream of the DC/DC converter and is therefore not directly comparable with the model voltage upstream of the converter ($RMSE^*_{off-rt} = 0.34\%$).

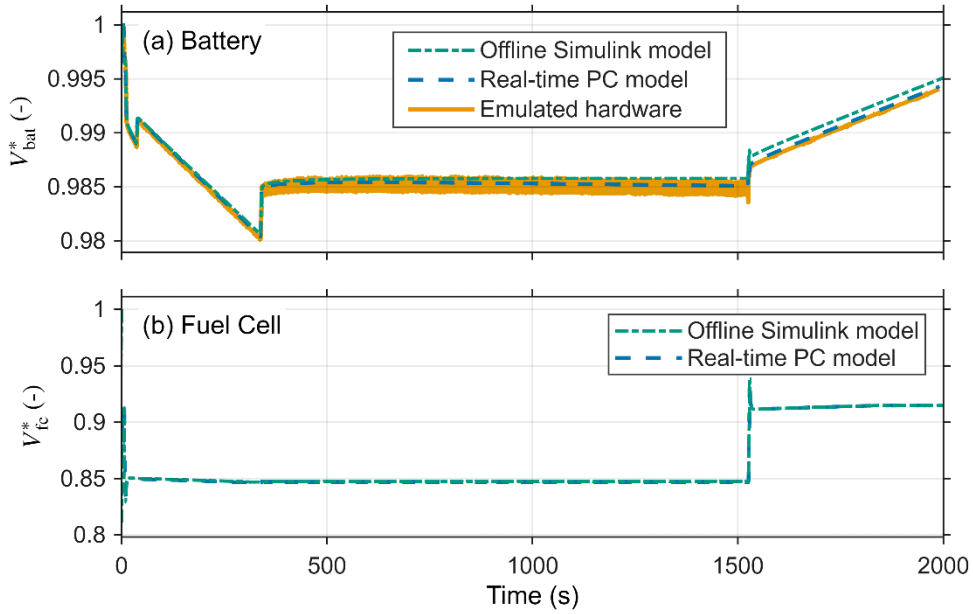


Figure 10 – Dimensionless voltage comparison during the standard mission: battery and fuel-cell subsystem.

The current response, in Figure 11, further highlights the power-sharing mechanism between the two sources. The fuel-cell current follows the commanded contribution generated by the EMS, while the battery current reflects the compensating action of the battery pack. The close agreement among the different signal sources indicates that the real-time model, the communication layer, and the power hardware are correctly synchronized for the considered mission dynamics ($RMSE^*_{off-rt} = 1.06\%\ and\ 0.90\%$, $RMSE^*_{rt-hw} = 0.25\%\ and\ 0.36\%$ for battery and fuel-cell, respectively).

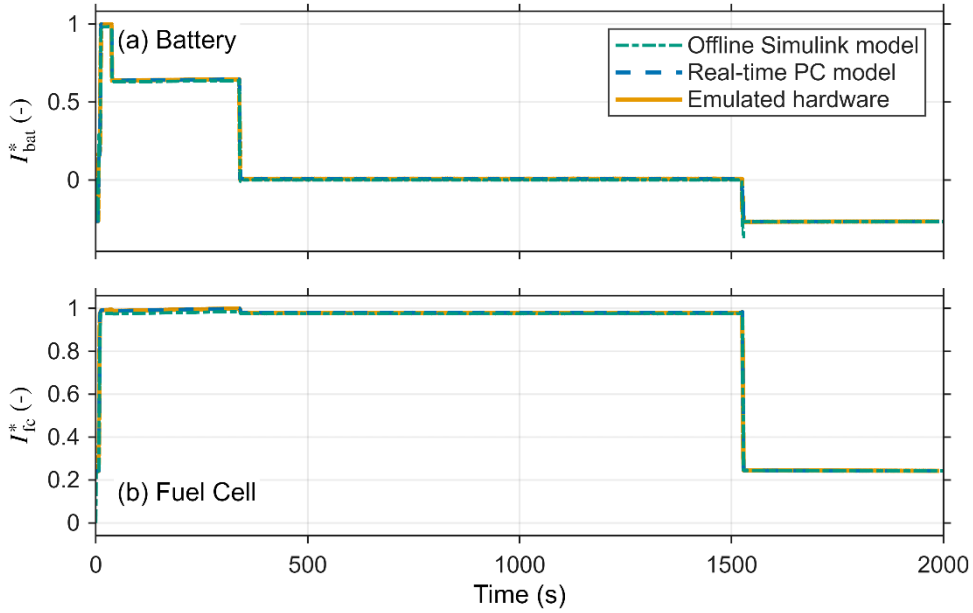


Figure 11 – Dimensionless current comparison during the standard mission: battery and fuel-cell subsystem.

Figure 12 shows the evolution of the battery state of charge and hydrogen consumption during the standard mission. The SoC trend is consistent with the expected role of the battery in nominal operation. During most of the mission, the fuel-cell provides the main power contribution, while the battery mainly compensates for transient power variations. In the final phase, however, the excess fuel-cell power available at idle operating conditions is redirected to the battery, producing a recharge phase. This is confirmed by the increase of the battery SoC observed in Figure 12, consistently with

the negative battery power shown in Figure 9. As expected, hydrogen consumption increases monotonically over the mission, reflecting the cumulative fuel usage associated with fuel-cell power production. A close agreement is observed between the offline and real-time implementations, yielding errors of $RMSE^*_{off-rt} = 0.21\%$ for the battery SoC and $RMSE^*_{off-rt} = 0.45\%$ for the hydrogen consumption. Overall, the standard mission confirms the capability of the proposed PHIL platform to emulate the nominal operation of a hybrid hydrogen-electric propulsion system.

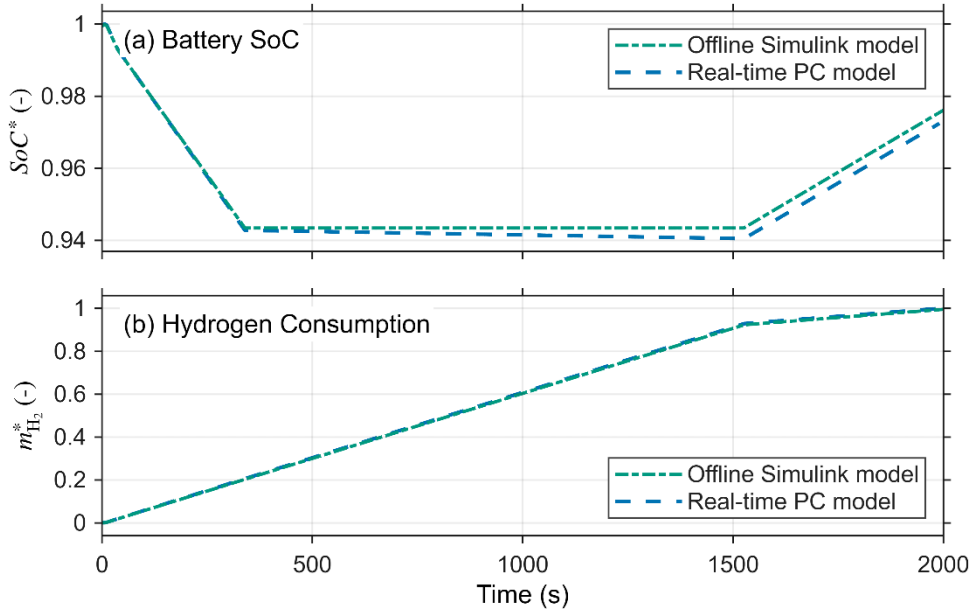


Figure 12 – Battery state of charge and hydrogen consumption during the standard mission.

6.2 Fuel-cell failure

The second mission investigates the behavior of the hybrid fuel-cell/battery powertrain under a degraded operating condition, in which a fuel-cell failure is introduced during the cruise phase. As described in Section 5, this scenario forces the energy management system to reconfigure the power split between the two sources, with the battery recovering the role of primary power source when the fuel-cell contribution is lost. This test case is therefore aimed at assessing both the robustness of the control strategy and the capability of the PHIL platform to reproduce fault-induced transients in a safe and repeatable environment.

Figure 13 shows the dimensionless power comparison during the fuel-cell failure mission. Before the fault occurrence, the system behavior is consistent with the standard mission: the fuel-cell supplies most of the load demand, while the battery provides transient support and compensates for the difference between the requested power and the fuel-cell contribution. The offline Simulink model, the real-time PC model, and the hardware emulator measurements show a good agreement, confirming the correct implementation of the nominal power-sharing logic in the real-time environment, with $RMSE^*_{off-rt} = 0.59\% \; and \; 0.54\%$, and $RMSE^*_{rt-hw} = 0.38\% \; and \; 0.21\%$ for the battery and the fuel-cell, respectively. At the failure event, occurring during the cruise phase, the fuel-cell power rapidly drops to zero. Consequently, the EMS reallocates the power demand to the battery, which becomes the main electrical source for the remaining cruise segment. This behavior is clearly visible in the battery power subplot, where the battery contribution increases immediately after the fuel-cell power loss. The transition is reproduced consistently by the offline model, the real-time PC model, and the emulator measurements, demonstrating that the PHIL platform is able to capture the abrupt redistribution of power caused by the fault condition.

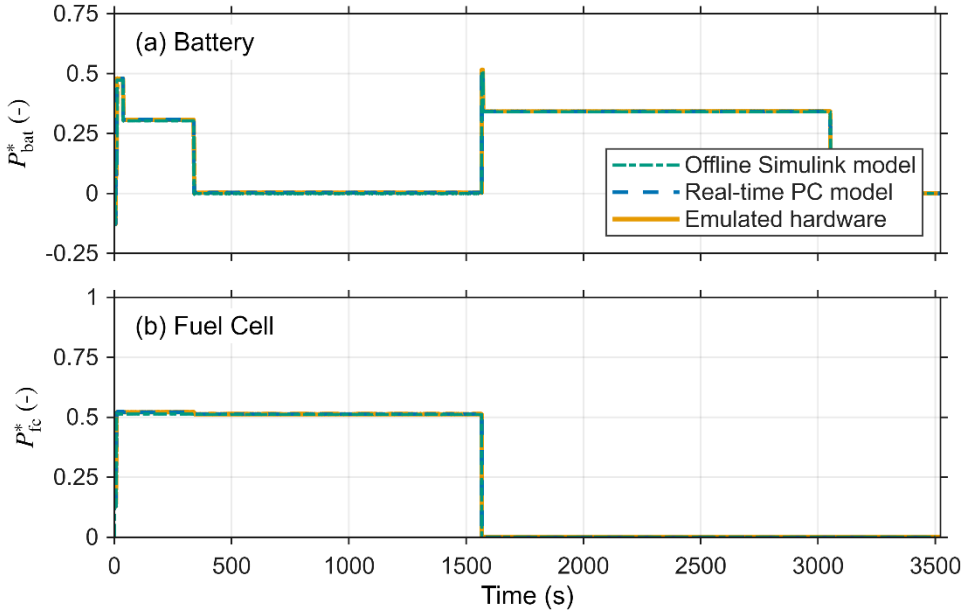


Figure 13 – Dimensionless power comparison during the fuel-cell failure mission: battery and fuel-cell subsystem

Figure 14 reports the corresponding voltage response. In the battery subsystem, the voltage follows the expected trend associated with the increased discharge demand after the fuel-cell failure. Once the battery becomes the primary source, the terminal voltage progressively decreases as a consequence of the higher current request and the resulting discharge process. The agreement between the offline model, the real-time PC model, and the hardware measurements remains satisfactory also after the fault, indicating that the battery emulator is able to reproduce the model-based voltage dynamics under degraded operating conditions ($RMSE^*_{off-rt} = 0.06\%$ *and* $RMSE^*_{rt-hw} = 0.03\%$). For the fuel-cell subsystem, the voltage comparison is limited to the offline Simulink model and the real-time PC model, since the available hardware voltage is measured downstream of the DC/DC converter and is therefore not directly comparable with the model voltage upstream of the converter ($RMSE^*_{off-rt} = 0.25\%$). After the failure, the fuel-cell current is forced to zero; consequently, the fuel-cell voltage response reflects the transition to a no-load or disconnected operating condition rather than active power generation.

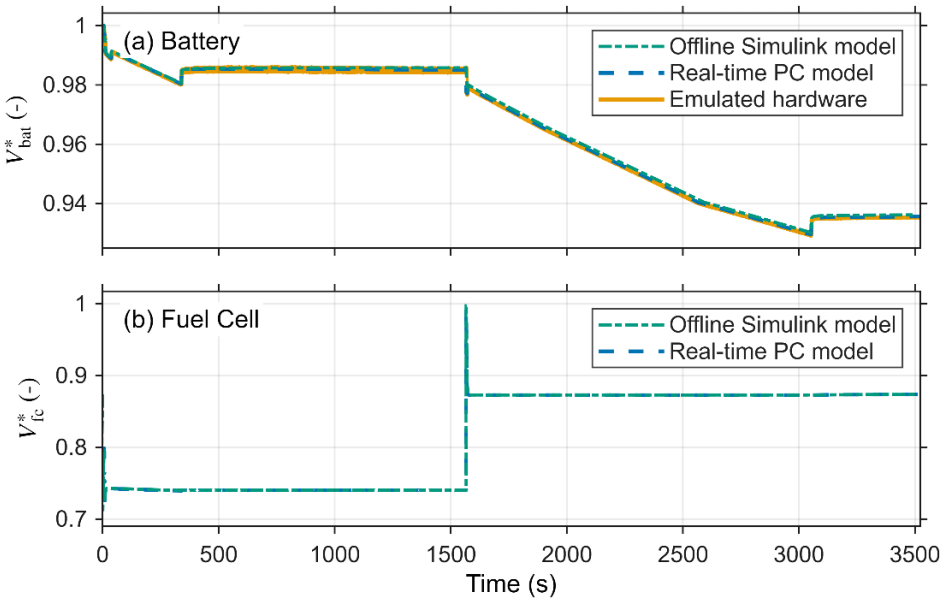


Figure 14 – Dimensionless voltage comparison during the fuel-cell failure mission: battery and fuel-cell subsystem.

The current response, shown in Figure 15, confirms the same reconfiguration mechanism. Before the failure, the fuel-cell current follows the commanded contribution generated by the EMS, while the battery current remains mainly associated with transient compensation. After the failure, the fuel-cell current decreases to zero, consistently with the loss of fuel-cell power. At the same time, the battery current increases and remains at a higher level during the rest of the cruise phase, confirming that the battery is required to sustain the load demand as the primary source. Small deviations between the curves can be attributed to sampling differences, communication delays, internal dynamics of the programmable DC units, and measurement filtering ($RMSE^*_{off-rt} = 0.80\% \; and \; 0.70\%$, $RMSE^*_{rt-hw} = 0.62\% \; and \; 0.34\%$ for battery and fuel-cell, respectively).

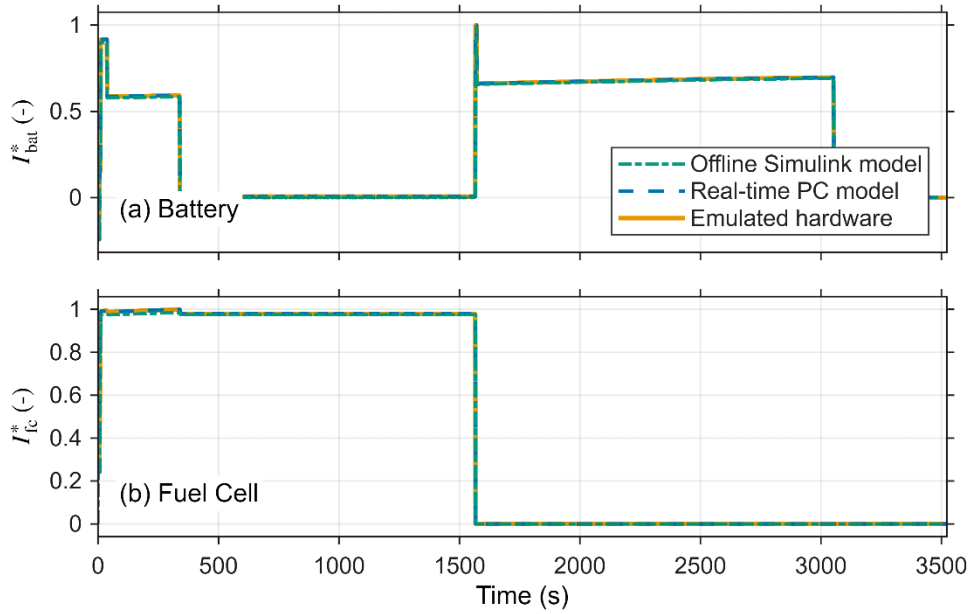


Figure 15 – Dimensionless current comparison during the fuel-cell failure mission: battery and fuel-cell subsystem.

Figure 16 shows the battery state of charge and hydrogen consumption during the fuel-cell failure mission. The SoC evolution is markedly different from the standard mission. Before the failure, the battery was mainly used as a buffer and its SoC variation remained limited. After the fuel-cell shutdown, the battery becomes the main source during cruise, leading to a more pronounced SoC decrease. This trend is consistent with power and current results ($RMSE^*_{off-rt} = 0.36\%$ for the battery SoC and $RMSE^*_{off-rt} = 0.52\%$ for the hydrogen consumption), where the battery contribution increases after the fault to compensate for the missing fuel-cell power. The hydrogen consumption increases during the initial part of the mission, when the fuel-cell is active and provides the main power contribution. After the failure event, the fuel-cell power and current drop to zero and the hydrogen consumption stabilizes, as the fuel-cell system no longer contributes to the load demand. This behavior confirms that the energy contribution is shifted from hydrogen to battery storage after the fault occurrence.

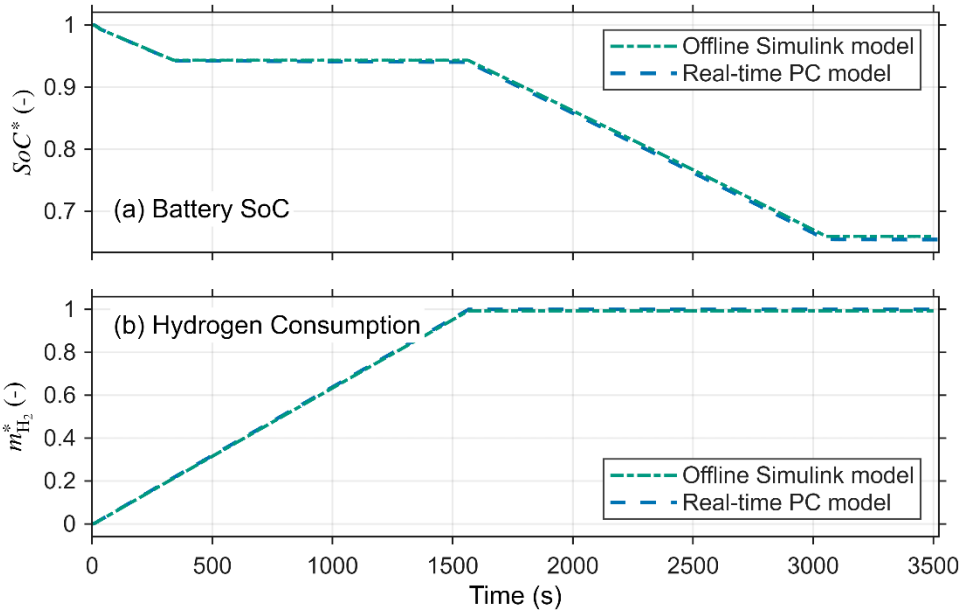


Figure 16 – Battery state of charge and hydrogen consumption during the fuel-cell failure mission.

Overall, the fuel-cell failure mission demonstrates the capability of the proposed PHIL platform to reproduce degraded operating conditions and to validate the EMS response under fault scenarios. The results show that the control strategy successfully reallocates the power demand to the battery when the fuel-cell contribution is lost, allowing the mission power request to be sustained during the remaining cruise phase. However, this fault-tolerant behavior is obtained at the cost of a faster battery discharge, as shown by the SoC evolution. The test therefore highlights the relevance of the platform for assessing energy management strategies, safety logic, and source reconfiguration mechanisms before the integration of real electrochemical devices.

7. Conclusion

This paper presented a Power-Hardware-in-the-Loop platform for the real-time emulation of a hybrid fuel-cell/battery electric propulsion system for aeronautical applications. The testbench integrates real-time Simulink models, energy management strategy, programmable DC power hardware, and a dedicated communication architecture to reproduce the dynamic interaction between a fuel-cell system, a battery pack, and an emulated propulsive load. The proposed architecture was validated through two representative mission profiles. In the standard mission, the fuel-cell acted as the primary energy source during cruise, while the battery provided transient support and power balancing. The comparison between the offline Simulink model, the real-time PC implementation, and the hardware emulator measurements showed good agreement in terms of power, voltage, and current response. This confirms that the real-time implementation and the programmable hardware units are able to reproduce the expected behavior of the hybrid powertrain under nominal operating conditions. The standard mission also highlighted the ability of the energy management strategy to handle low-load conditions. In the final phase of the mission, the requested load power decreased below the minimum idle operating power of the fuel-cell. Instead of switching off the fuel-cell system, the EMS maintained it at its minimum stable operating level and redirected the surplus power to the battery. This resulted in negative battery power, according to the adopted sign convention, and in a corresponding increase of the battery state of charge. A second mission was used to assess the platform response under a fuel-cell failure scenario. After the fault occurrence, the fuel-cell power and current dropped to zero and the EMS reallocated the load demand to the battery, which became the main power source during the remaining cruise segment. The results showed that the platform can reproduce fault-induced transients and source reconfiguration mechanisms in a controlled and repeatable laboratory environment. The faster decrease of the battery state of charge after the failure confirmed the increased energy contribution required from the battery when the fuel-cell system is unavailable.

Overall, the results demonstrate that the proposed PHIL test bench is suitable for validating real-time models, communication interfaces, programmable power hardware, and energy management strategies for hybrid hydrogen-electric propulsion systems. The platform provides a flexible and safe environment for testing nominal and degraded operating conditions before the integration of real electrochemical sources.

Future work will focus on the integration of real fuel-cell and battery hardware, the extension of the experimental campaign to additional fault scenarios, and the inclusion of more advanced energy management strategies. Further developments will also address higher-fidelity component models and the validation of the platform at higher power levels representative of scalable aeronautical applications.

8. Contact Author Email Address

Gianluca Marinaro: G.Marinaro@cira.it

Luca Garbarino: L.Garbarino@cira.it

9. Copyright Statement

The authors confirm that they, and/or their company or organization, hold copyright on all of the original material included in this paper. The authors also confirm that they have obtained permission, from the copyright holder of any third party material included in this paper, to publish it as part of their paper. The authors confirm that they give permission, or have obtained permission from the copyright holder of this paper, for the publication and distribution of this paper as part of the ICAS proceedings or as individual off-prints from the proceedings.

References

[1] B. de V. Leitão, C. Bringhenti, J. T. Tomita, F. J. dos Santos Silva, C. Xisto, and T. Grönstedt, “A review of hydrogen aircraft propulsion systems: recent advances and environmental perspectives,” Int J Hydrogen Energy, vol. 176, p. 151489, Oct. 2025, doi: 10.1016/J.IJHYDENE.2025.151489.

[2] T. H. Bradley, B. A. Moffitt, D. E. Parekh, T. F. Fuller, and D. N. Mavris, “Energy management for fuel cell powered hybrid-electric aircraft,” 7th International Energy Conversion Engineering Conference, 2009, doi: 10.2514/6.2009-4590.

[3] R. Ma, C. Liu, Z. Zheng, F. Gechter, P. Briois, and F. Gao, “CPU-FPGA based real-time simulation of fuel cell electric vehicle,” Energy Conversion and Management, vol. 174, pp. 983–997, 2018, doi:10.1016/j.enconman.2018.08.099.

[4] Y. Zhou, A. Ravey, and M.-C. Péra, “Real-time cost-minimization power-allocating strategy via model predictive control for fuel cell hybrid electric vehicles,” Energy Conversion and Management, vol. 229, p. 113721, 2021, doi:10.1016/j.enconman.2020.113721.

[5] V. Pizarro-Carmona, S. Castano-Solís, M. Cortés-Carmona, J. Fraile-Ardanuy, and D. Jimenez-Bermejo, “GA-based approach to optimize an equivalent electric circuit model of a Li-ion battery-pack,” Expert Systems with Applications, vol. 172, p. 114647, 2021, doi:10.1016/j.eswa.2021.114647.

[6] P. H. J. Kleutgens et al., “A power hardware-in-the-loop test bench for emulation of test scenarios and mission profiles for high-power DC charging stations,” e+i Elektrotechnik und Informationstechnik 2024 142:1, vol. 142, no. 1, pp. 30–41, Dec. 2024, doi: 10.1007/S00502-024-01300-2.

[7] J.-H. Jungy, “Real-time and power hardware-in-the-loop simulation of PEM fuel cell stack system” Journal of Power Electronics. 11. 202-210, 2011.

[8] H. Zhang, Y. Zhai, X. Yang, S. Liu, X. Wang, and S. Shuai, “Energy management strategy for parallel hybrid electric aircraft considering SOC sustainment,” Energy, vol. 339, p. 138940, 2025, doi:10.1016/j.energy.2025.138940.

[9] J. Sachs-Wetstone, S. Bianco, J. L. Kratz, M. Horning, A. E. Amthor, and J. W. Connolly, “Hybrid-Electric Aero-Propulsion Controls Testbed Results,” in AIAA AVIATION 2023 Forum, 2023, doi:10.2514/6.2023-4233

[10] A. Movahedian, G. Marinaro and E. Frosina, "Numerical Assessment of Hybrid PEMFC-Battery vs. Battery-Only Propulsion for Sustainable Light Aviation," in Journal of Physics: Conference Series, vol. 3143, no. 1, p. 012087, Dec. 2025, doi: 10.1088/1742-6596/3143/1/012087

[11]P. Kollmeyer and M. Skells, "Samsung INR21700 30T 3Ah Li-ion Battery Data," Mendeley Data, vol. 2, 2023, doi: 10.17632/9xyvy2njj3.2

[12]A.-I. Stroe, J. Meng, D.-I. Stroe, M. J. Swierczynski, R. Teodorescu and S. K. Kær, "Influence of Battery Parametric Uncertainties on the State-of-Charge Estimation of Lithium Titanate Oxide-Based Batteries," in Energies, vol. 11, no. 4, Art. no. 795, pp. 1-19, 2018, doi: 10.3390/en11040795

[13]N. Zatta, B. De Cesaro, E. Dal Cin, G. Carraro, G. Cristofoli, A. Trovò, A. Lazzaretto and M. Guarnieri, "Holistic Testing and Characterization of Commercial 18650 Lithium-Ion Cells," in Batteries, vol. 10, no. 7, Art. no. 248, 2024, doi: 10.3390/batteries10070248

[14]L. Mattia, H. Beiranvand, W. Zamboni, and M. Liserre, “Lithium-ion battery thermal modelling and characterization: A comprehensive review,” Journal of Energy Storage, vol. 129, p. 117114, 2025, doi: 10.1016/j.est.2025.117114.

[15]M. S. Munsi and H. Chaoui, "Energy Management Systems for Electric Vehicles: A Comprehensive Review of Technologies and Trends," in IEEE Access, vol. 12, pp. 60385-60403, 2024, doi: 10.1109/ACCESS.2024.3371483.